SUPPLEMENTAL MATERIAL

Adenosine-Induced Atrial Fibrillation: Localized Reentrant Drivers in Lateral Right Atria due to Heterogeneous Expression of Adenosine A1 Receptors and GIRK4 Subunits in the Human Heart

Li et al.: Adenosine and Atrial Fibrillation

Authors: Ning Li, MD, PhD[1,2]; Thomas A. Csepe, BS[1,2]; Brian J. Hansen, BS[1,2]; Lidiya V. Sul[1,2]; Anuradha Kalyanasundaram, PhD[1,2]; Stanislav O. Zakharkin, PhD[1]; Jichao Zhao, PhD[3]; Avirup Guha, MD[1,4]; David R. Van Wagoner, PhD[5]; Ahmet Kilic, MD[2,4,6]; Peter J Mohler, PhD[1,2,4]; Paul ML Janssen, PhD[1,2,4]; Brandon Biesiadecki, PhD[1,2]; John D Hummel, MD[2,4,6]; Raul Weiss, MD [2,4,6]; Vadim V. Fedorov, PhD [1,2]

Affiliations: 1- Department of Physiology & Cell Biology, The Ohio State University Wexner Medical Center, Columbus, OH, USA

2- Davis Heart & Lung Research Institute, The Ohio State University Wexner Medical Center, Columbus, OH, USA

3- Auckland Bioengineering Institute, The University of Auckland, Auckland, New Zealand

4- Department of Internal Medicine, The Ohio State University Wexner Medical Center, Columbus, OH, USA

5- Department of Molecular Cardiology, Cleveland Clinic, Cleveland Ohio, USA

6- Department of Surgery, Division of Cardiac Surgery, Wexner Medical Center, The Ohio State University, Columbus, OH.

Address for correspondence: Vadim V. Fedorov, PhD

Department of Physiology and Cell Biology, The Ohio State University Wexner Medical Center

300 Hamilton Hall, 1645 Neil Avenue, Columbus OH 43210-1218

tel: 1-614-292-9892 fax: 1-614-292-4888

e-mails: vadim.fedorov@osumc.edu, fedorov.2@osu.edu

Supplemental Methods

Optical mapping of coronary-perfused atrial preparations

Explanted human hearts were obtained from The Ohio State University Cardiac Transplant Team and LifeLine of Ohio in accordance with The Ohio State University Institutional Review Board. Human hearts (n=37) were obtained in the operating room at the time of cross-clamp and immediately preserved with ice-cold cardioplegic solution and stored at 4°C during transport and dissection. Hearts were transported to the experimental lab within 15 minutes and coronary-perfused with oxygenated cardioplegic solution at 4°C to prevent any potential tissue degradation[1-3]. Human atrial tissue was utilized for optical mapping experiments (n=24, **Supplemental Table I**) and/or multi-regional immunoblotting analysis (n=18, **Supplemental Table II**).

Human atrial preparations (n=24) were isolated and coronary-perfused as previously described[4]. In nine of the atrial preparations, bi-atrial optical mapping[2] of the whole atria from epicardium (epi) was performed (**Figure 1 and Figure 5**). In the remaining 15 hearts, the pulmonary veins region, including part of the interatrial septum, was kept by the surgical team for cardiac and/or lung transplantation. As such, endocardial (endo) or epi optical mapping was performed on preparations containing both lateral LA and RA (n=2, **Figure 2**) or only RA (n=6)[1, 4]. Simultaneous dual-sided optical mapping[1] was utilized on isolated LA (n=2) and RA (n=5) to examine the APD response of sub-epi tissue vs. sub-endo tissue to adenosine. All mapped preparations excluded regions of poor coronary perfusion/ischemia.

After 40-70 minutes of washout with oxygenated Tyrode's solution and warming to 37°C to ensure tissue recovery and stabilization, the human atrial preparations were immobilized by perfusion with 10μM blebbistatin and stained with near-infrared dye di-4-ANBDQBS (10-40μM)[5].

Imaging was simultaneously conducted with two (n=19) to four (n=3) MiCAM Ultima-L CMOS cameras (SciMedia, Ltd., CA USA) from atrial epi and/or endo fields of view (330-940μm^2 resolution, 100×100 pixels), sampled at 1000 frames/s. The fluorescent signals were amplified, digitized, and visualized during the experiments[6]. The preparations were instrumented with two customized bipolar pacing electrodes placed on the RA or LA epi or endo surface. Electrical activity was continuously recorded from a 2mm bipolar sensing catheter (7Fr, 8mm tip, Biosense Webster, CA) placed on the atrial epi or endo surface, and a far-field pseudo atrial ECG was recorded by two Ag–AgCl plaque electrodes (9-mm diameter).

Following motion suppression with 10μM blebbistatin and staining with near-infrared dye di-4-ANBDQBS (10-40μM)[5], preparations were equilibrated for 20–30 min before imaging. Atrial preparations (n=19) were sequentially imaged during perfusion by regular Tyrode's solution (baseline), 10μM and/or 100μM adenosine (Sigma MO, USA) followed by the selective GIRK channel blocker tertiapin (10-100nM) (Tocris Bristol, UK) or washout. In five of the preparations, 100μM adenosine was added after 100nM tertiapin perfusion. The time interval between drug applications was 20-30 minutes. In all whole atrial preparations, sinus rhythm was recovered prior to pacing protocol. All preparations were paced at a basic cycle length (CL) of 500ms, and paced incrementally until the functional refractory period was reached or AF was induced[1, 4]. This restitution pacing protocol was repeated after drug application. Additionally, burst pacing with a CL faster than the functional refractory period was used to induce AF.

All optical mapping data were analyzed by a customized Matlab program as previously described[1, 7]. Activation maps and conduction velocity were constructed from activation times, which were determined from maximum upstroke of OAPs (dV/dt max) for each channel. Atrial activation patterns and 80% of repolarization (APD80) were analyzed at baseline and during adenosine, and tertiapin perfusion. APD changes were compared using recordings taken at 2-5

minutes after adenosine perfusion and 15-20 minutes after tertiapin perfusion, when the maximum drug effects were reached. Activation frequency of RA and LA during AF was measured with dominant frequency (DF) analysis and discrete islands of highest DF were considered AF driver regions, which were limited to 2.5x2.5cm^2 regions[1,2,7](**Figure 3**). Additionally, activation maps (**Figures 3-5**) and movies were used to identify the mechanism of AF reentrant drivers[1]. Here, AF drivers are defined as a localized source(s) of fastest electrical activity visualized as reentrant circuits where two pivot points were mapped or breakthrough pattern and incomplete reentry circuits where one pivot point was mapped that were temporally stable for >70% of the AF duration if only one driver was seen or >30% if two drivers were seen. The temporal stability of the AF driver is estimated by the percentage of activation cycles with activation source origin within a driver region during 8 seconds recording. Based on our previous transmural mapping study[1], we suggest that the incomplete reentry or stable breakthrough visualized in the present study by single-sided mapping is intramural reentry, and this pattern is referred to as incomplete reentry/breakthrough (**Supplemental Figure I**). Breakthroughs distributed within 1x1 cm^2 area of the driver region during an AF episode are defined as spatially stable breakthroughs. Breakthroughs distributed between 1x1cm^2 and 2.5x2.5cm^2 area of the driver region are defined as spatially unstable breakthroughs from one single driver.

Immunobloting

In thirteen hearts, fresh atrial tissue was collected and flash-frozen in liquid nitrogen during heart dissection from different atrial locations in order to study the A1R and GIRK1/4 protein expression. The location of the collected tissue included LA and RA appendages, lateral LA, posterior LA/inferior pulmonary veins, interatrial septum, crista terminalis, superior, middle and inferior lateral RA (pectinate muscle regions), and RA base (vestibule) as shown in **Figure 6**. In another five hearts, the atrial tissue was collected from the tip of both appendages and the edge

of LA and RA lateral wall before optical mapping to confirm the direct correlation of functional and molecular data. Protein isolation and immunoblotting were performed by methods previously described[3, 7, 8]. Primary antibodies against A1R (1:500; Abcam), GIRK1 (1:500; Alomone, Israel), GIRK4 (1:500; Alomone, Israel) and GAPDH (1:10000, Sigma) were used to quantify corresponding proteins in atrial tissue homogenates[7]. Cy5 conjugated goat anti-rabbit (1:2000, Jackson) was used as secondary antibody. The specific bands were detected on a Typhoon 9410 imager (GE Healthcare) and quantified by densitometry analysis (ImageQuant, GE Healthcare). Based on previous publications[7, 9, 10], specific bands at the expected molecular weights for A1R (~37kDa), GIRK4 (~50kDa) and GIRK1 (~65kDa) proteins were detected. A1R, GIRK1, and GIRK4 protein expression was normalized to GAPDH.

Ex vivo Micro-Computed Tomographic Imaging

We conducted detailed 3D structural analysis on the functionally mapped human atria, with emphasis on atrial structures that harbor localized drivers, using iodine-enhanced Micro-Computed Tomographic Imaging (micro-CT) for high-resolution imaging of atrial anatomy[11]. After functional mapping, the human atrial tissue was formalin fixed for 24 hours, then washed out with PBS and incubated at 4°C in 25% Lugol iodine solution for 6 days[12]. Whole atria or specific AF driver locations were imaged by a micro PET-CT (Inveon, Siemens) scanner to acquire a resolution of 20x20x20 μm^3 with a 2x4x4 cm^3 field of view (AF driver area). Structure-tensor analysis was used to characterize atrial fibers from the 3D atrial volume, as iodine preferentially accumulates within the muscular fibers rather than in connective tissues. **Supplemental Figure II** shows results from our experiment in which we scanned the main AF driver region from Heart #10 and revealed complex myofiber structures that play a critical role in anchoring reentrant arrhythmias. These data show our ability to quantitatively measure and analyze 3D atrial anatomy and fiber orientations together with complex AF activation/conduction patterns within the human atria.

Statistical Analysis

Data are presented as mean ± SD other than AF episode duration, which is presented as mean ± SEM. Comparison of measurements within each heart (LA vs. RA and between treatment conditions), was done using PROC MIXED in SAS 9.4 (SAS institute, Cary, NC) with group or treatment as a fixed factor and heart ID as a random factor. Pairwise comparisons were done with Tukey's adjustment, which is commonly used and has been recommended for Circulation papers[13]. Comparisons of inducible vs. non-inducible and failing vs. non-failing hearts were done in R 3.2.3 using an independent groups two-sided t-test or non-parametric Wilcoxon test based on whether normality assumptions were met according to Anderson-Darling test. P-values of 0.05 or below were considered significant.

Supplemental Tables

Supplemental Table I. Human heart information for optical mapping experiments

Heart No.	Case No.	Age	Sex	AF	HF	Main Diagnoses	Device	H.W. (g)
1	947202	34	M	-	-	Head Trauma, Drug Abuse	None	446
2	442404	69	M	-	-	CVA/ICH, DM, HTN	None	659
3	257102	43	F	-	-	CVA/ICH, COPD	None	329
4	266541	57	M	-	-	ICB/ICH, DM	None	635
5	402879	54	M	-	-	ICB/ICH, HTN	None	474
6	984478	54	F	-	-	ICB/ICH, HTN	None	348
7	481041	41	M	-	-	CVA/ICH, HTN	None	455
8	118258	38	M	-	-	CVA/ICH, HTN	None	575
9	474083	41	F	-	-	CVA, HTN	None	-
10	522421	56	F	-	+	Non-Ischemic HF (Transplant), Stroke, VT	ICD	470
11	240603	51	F	-	-	Blunt Head Trauma, HTN	None	320
12	685884	36	M	-	-	Cardiac Arrest, HTN	None	415
13	749693	65	M	-	-	CVA/ICH, HTN	None	643
14	450564	30	M	+	+	Non-Ischemic HF (Transplant), Atrial Flutter	ICD	482
15	479062	50	M	-	+	Ischemic HF (Transplant), VT	ICD	636
16	537114	48	M	-	+	Non-Ischemic HF (Transplant)	ICD, LVAD	439
17	323104	63	M	-	+	Non-Ischemic HF (Transplant), HTN	CRT	543

18	328163	63	M	-	+	Ischemic HF (Transplant)	ICD	506
19	728878	40	M	-	+	Non-Ischemic HF (Transplant)	LVAD, PM	747
20	380071	43	F	-	-	Respiratory Arrest, CAD, HTN, DM	None	603
21	645444	47	M	-	+	Ischemic HF (Transplant)	LVAD	411
22	963542	60	F	-	+	Non-Ischemic HF (Transplant)	ICD	329
23	422358	52	M	-	+	Ischemic HF (Transplant)	LVAD	498
24	514489	42	F	-	-	Cardiac Arrest	None	327

Abbreviations: AF = Atrial fibrillation; CAD = Coronary artery disease; CRT = Cardiac resynchronization therapy; CVA/ICH = Cardiovascular attack/Intracranial hemorrhage; DM = Diabetes mellitus; HF = Heart failure; HTN = Hypertension; H.W. = Heart weight; ICD = Implantable cardiac defibrillator; LVAD = Left ventricular assist device; PM = Pacemaker; VT = Ventricular tachycardia.

Supplemental Table II. Human heart information for molecular mapping experiments

Heart No.	Case No.	Age	Sex	AF	HF	Main Diagnoses	Device	H.W. (g)
*1	947202	34	M	-	-	Head Trauma, Drug Abuse	None	446
*2	442404	69	M	-	-	CVA/ICH, DM, HTN	None	659
*10	522421	56	F	-	+	Non-Ischemic HF (Transplant), Stroke, VT	ICD	470
*12	685884	36	M	-	-	Cardiac Arrest, HTN, Drug/Alcohol Abuse	None	415
*18	328163	63	M	-	+	Ischemic HF (Transplant)	ICD	506
25	911614	65	M	+	+	Non-Ischemic HF (Transplant), AF	CRT, LVAD	716
26	774694	50	F	-	+	Ischemic HF (Transplant), CAD	None	486
27	674541	64	M	+	+	Stroke, CAD, HF, DM, HTN, AF	ICD, LVAD	599
28	600245	51	F	-	-	CVA/ICH	None	507
29	809108	60	M	-	-	Cardiac Arrest, HTN,DM	None	842
30	147381	58	M	+	-	Blunt Injury, CAD, HTN, AF	None	512
31	768159	44	M	-	-	Cardiac Arrest, DM, VF	None	279
32	380071	43	F	-	-	Respiratory Arrest, HTN, DM, COPD, CAD, MI	None	603
33	712301	67	M	-	-	Blunt Injury, HTN	None	527
34	845013	26	M	-	-	Cardiac Arrest, VSD, VF, VT	PM	497
35	724569	64	M	+	+	Non Ischemic HF(Transplant), AF, VT, HTN	ICD	636
36	971258	57	M	+	+	Ischemic HF(Transplant), CAD,	LVAD, ICD	619

						MI, AF		
37	574165	62	M	+	-	Blunt Injury, Drug/Alcohol abuse, AF	None	584

Abbreviations: VF = Ventricular fibrillation; VSD = Ventricular septal defect. Other abbreviations as seen in **Supplemental Table I**. * denotes that heart was used for both optical and molecular mapping.

Supplemental Table III. Adenosine effect on right atrial APD in failing vs non-failing hearts

	Average APD (ms) (% APD shortening)			Minimum APD (ms) (% APD shortening)		
	Baseline	Ado10	Ado100	Baseline	Ado10	Ado100
HF (n=8)	295±38	241±43 (14.3%)	244±42 (16.8%)	288±36	227±55 (17.1%)	237±47 (16.9%)
NF (n=13)	287±50	249±32 (14.7%)	218±38 (18.4%)	279±48	236±32 (16.9%)	207±37 (20.9%)

Abbreviations: Ado10 = Adenosine 10μM; Ado100 = Adenosine 100μM; APD = Action potential duration 80%; HF = Heart failure; NF = Non-failing

Supplemental Figures and Figure Legends

Supplemental Figure I.

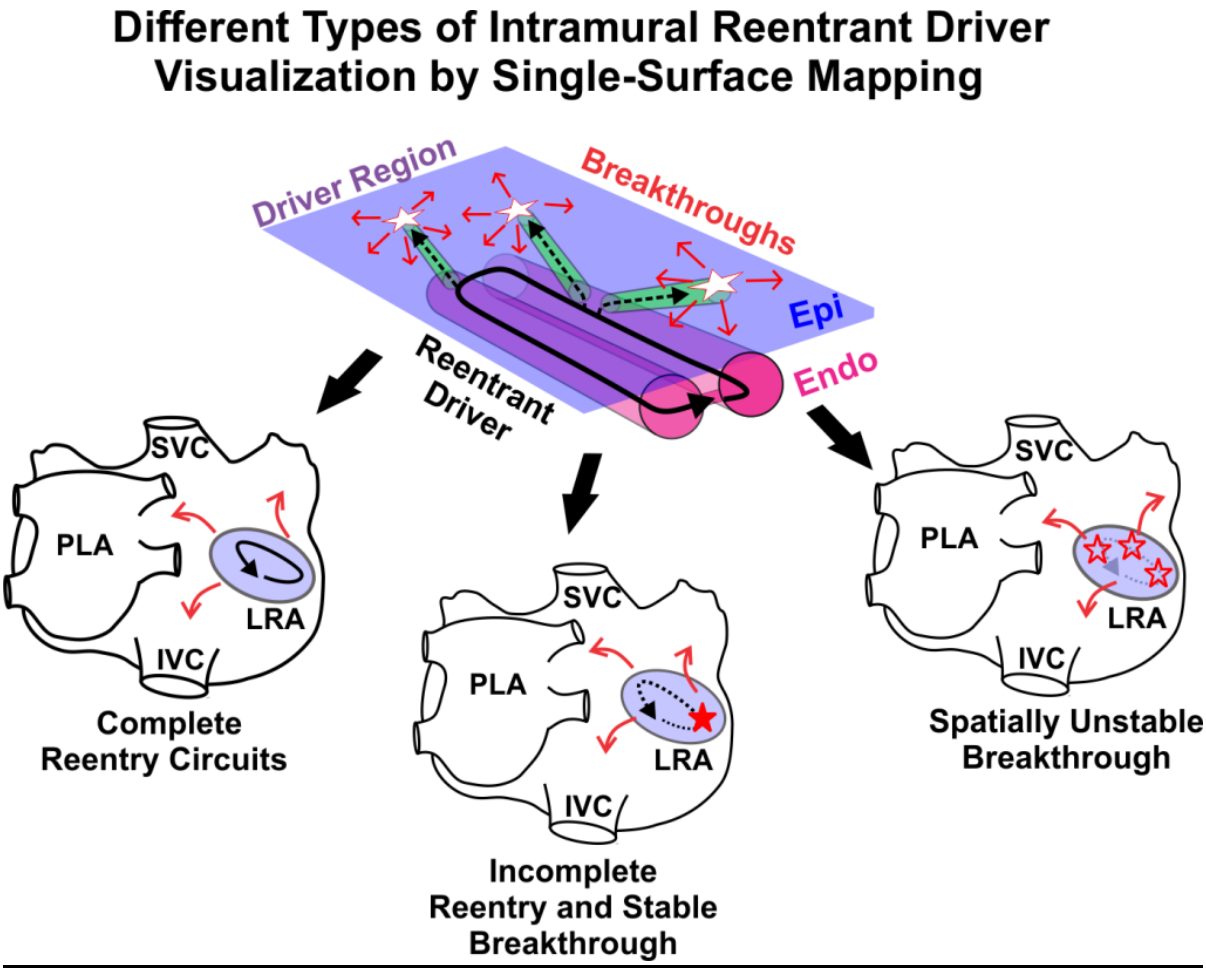

Based on our dual-sided optical mapping study[1], different types of intramural reentrant driver visualization by single-surface mapping exist: 1) complete reentry circuits, 2) incomplete reentry circuits and spatially stable breakthrough, and 3) spatially unstable breakthrough. Abbreviations: Epi - epicardium; Endo - endocardium; IVC- inferior vena cava; LRA - lateral right atria; PLA - posterior left atria; SVC – superior vena cava.

Supplemental Figure II. Spatially and temporally stable incomplete reentry circuits/breakthrough driving adenosine-induced AF in human Heart #1 (947202) from Figure 3.

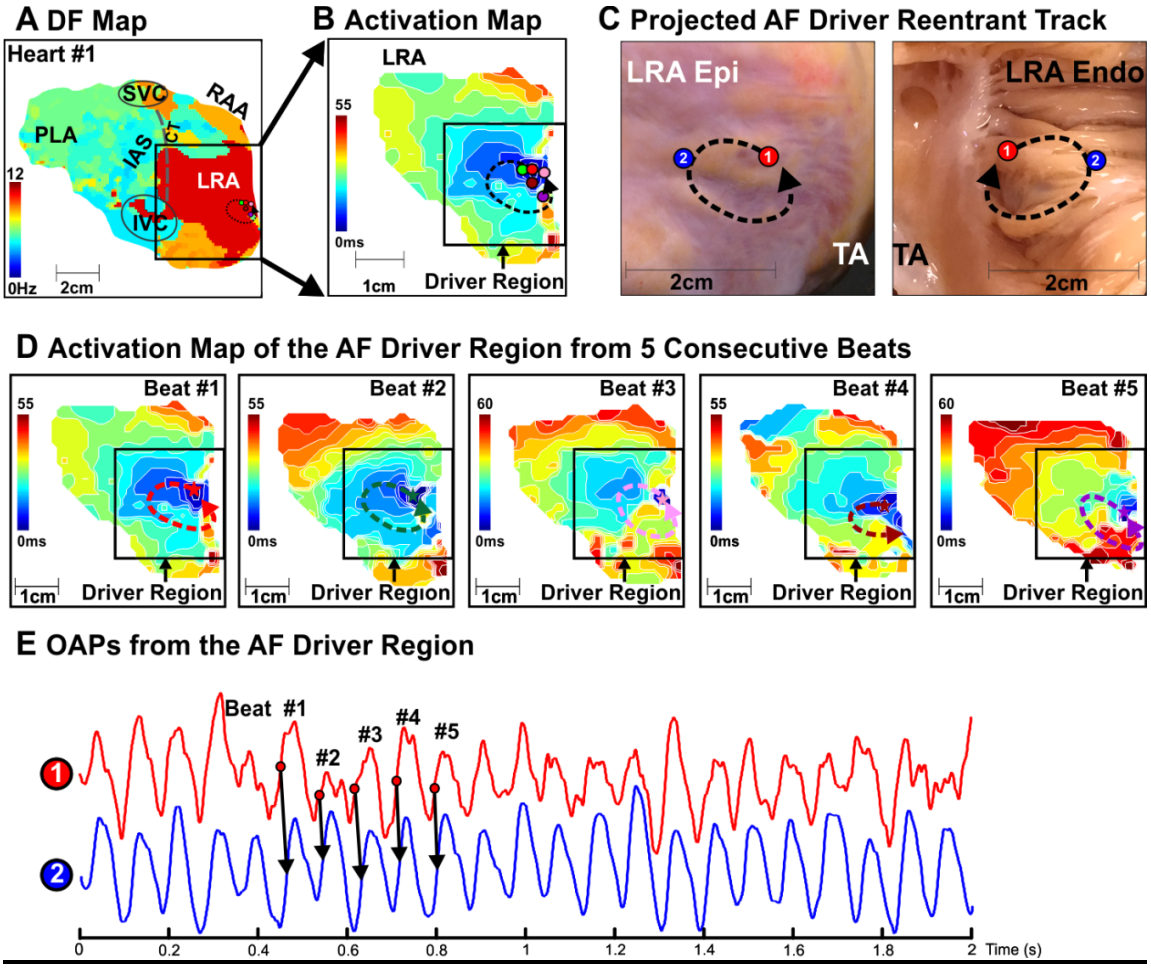

A, Dominant frequency (DF) map during 100μM adenosine-induced AF. **B**, Activation map of the driver region in the lateral right atria (LRA). The colored dots indicate the mapped breakthrough locations for beats 1-5 shown in panel **D**. Dashed arrow shows the projected reentry circuit of the AF driver. **C**, The anatomy of the projected AF driver reentrant track along pectinate muscles. **D**, Activation maps of the AF driver region from 5 consecutive beats during adenosine-induced AF. **E**, Optical action potentials (OAPs) from the AF driver region. Abbreviations as in **Supplemental Figure I**; AF - atrial fibrillation; CT- crista terminalis; DF - dominant frequency; IAS- intra-atrial septum.

Supplemental Figure III. Spatially and temporally stable reentry driving adenosine-induced AF in human Heart #10 (522421) from Figure 4.

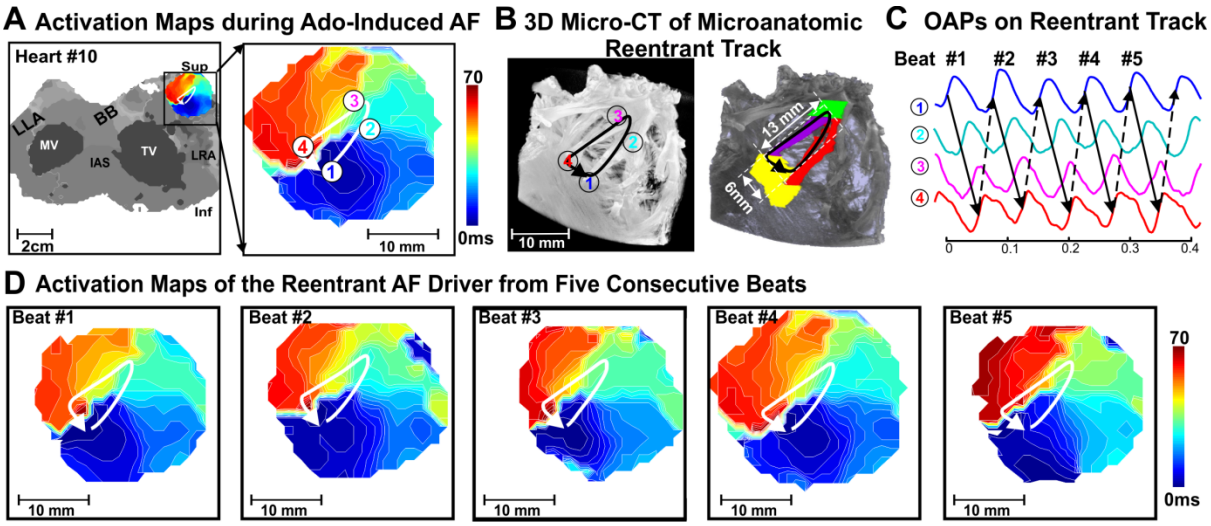

A, Activation map during 10μM adenosine-induced AF. Arrow shows the reentry circuit of the AF driver. **B**, Micro-CT revealed sub-endocardial structure of the microanatomic AF driver track in the superior lateral right atria (LRA). **C**, Optical action potentials on the reentry track from the location indicated by colored numbers in panel **A** and **B**. **D**, Activation maps showing stability of reentrant AF driver during 5 consecutive beats. Abbreviations as in **Supplemental Figure I.**

Supplemental Figure IV. Conduction velocity of the reentrant AF driver in Heart #10 (522421) from Figure 4.

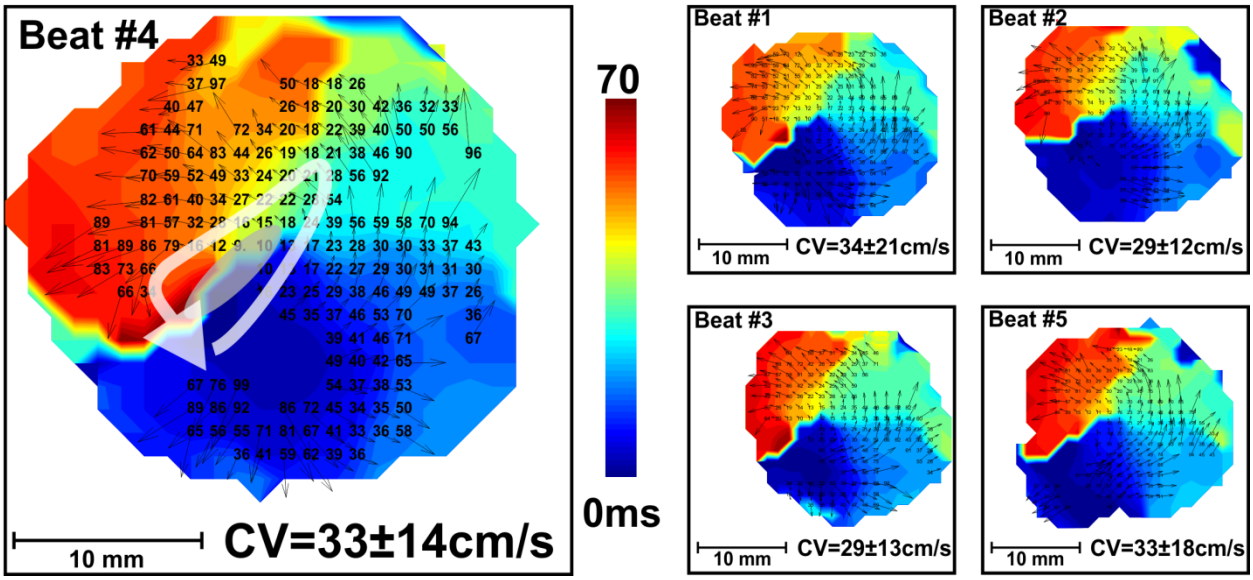

Activation maps showing conduction velocity of the AF reentrant circuit in Heart #10 (522421) for five consecutive beats. Small black numbers and arrows indicate local conduction velocity and direction. White arrow indicates reentrant track shown in **Supplemental Figure III**. Grey oval indicates region of slow conduction at center of reentrant track. Numbers at bottom right of activation maps show the average conduction velocity and standard deviation along the reentrant track. Abbreviations as in **Supplemental Figure I**; CV - conduction velocity.

Supplemental Figure V. APD analysis in driver regions during adenosine-induced AF.

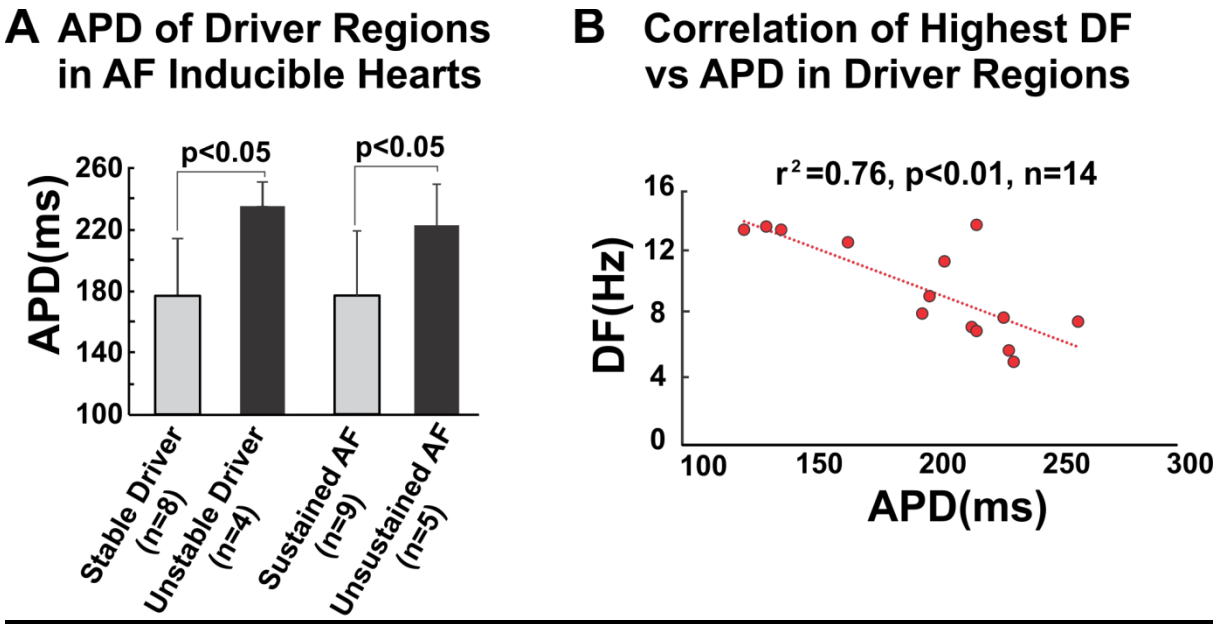

A, The APD of stable driver regions is shorter than APD in unstable driver regions and the APD in driver regions of sustained AF is shorter than that of unsustained AF. See Table 1 for driver characteristics. **B**, The correlation of highest DF vs APD in driver regions.

Supplemental Figure VI. Right to left atrial expression ratio of A1R and GIRK4 proteins.

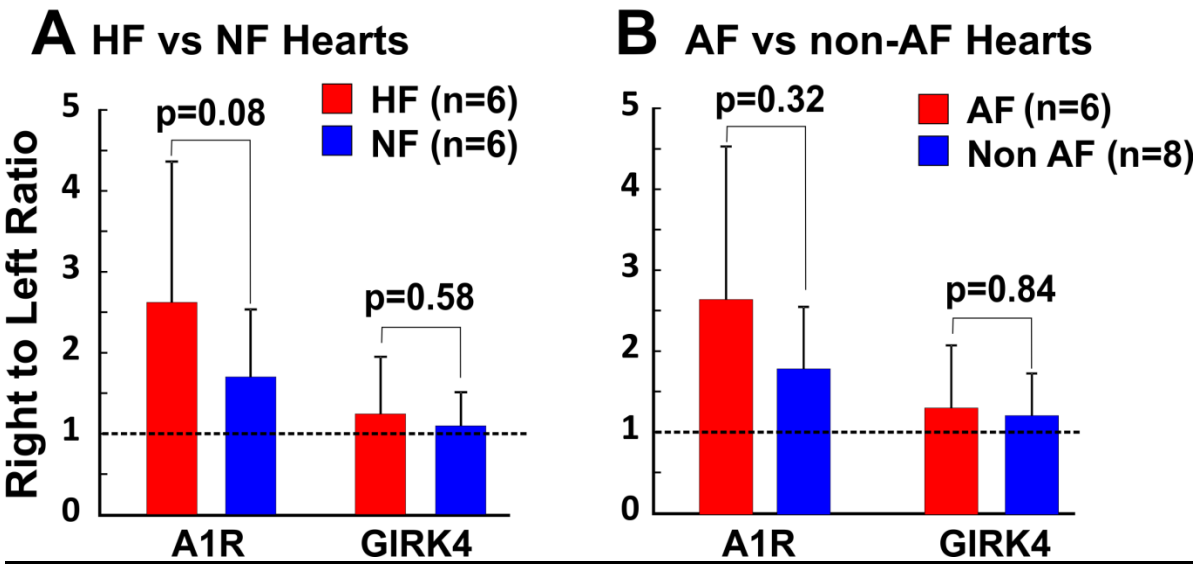

A, Immunoblot of A1R and GIRK4 protein in LA and RA from failing vs non-failing and non-AF hearts. **B**, AF vs non-AF and non-failing hearts. GAPDH normalized band density is shown in mean±SD and normalized to the value of the lateral left atria. See **Figure 7** for more details.

Supplemental References

1. Hansen BJ, Zhao J, Csepe TA, Moore BT, Li N, Jayne LA, Kalyanasundaram A, Lim P, Bratasz A, Powell KA, Simonetti OP, Higgins RS, Kilic A, Mohler PJ, Janssen PM, Weiss R, Hummel JD, Fedorov VV. Atrial fibrillation driven by micro-anatomic intramural re-entry revealed by simultaneous sub-epicardial and sub-endocardial optical mapping in explanted human hearts. *Eur Heart J.* 2015;36:2390-2401.

2. Zhao J, Hansen BJ, Csepe TA, Lim P, Wang Y, Williams M, Mohler PJ, Janssen PM, Weiss R, Hummel JD, Fedorov VV. Integration of High-Resolution Optical Mapping and 3-Dimensional Micro-Computed Tomographic Imaging to Resolve the Structural Basis of Atrial Conduction in the Human Heart. *Circ Arrhythm Electrophysiol.* 2015;8:1514-1517.

3. Li N, Csepe TA, Hansen BJ, Dobrzynski H, Higgins RS, Kilic A, Mohler PJ, Janssen PM, Rosen MR, Biesiadecki BJ, Fedorov VV. Molecular Mapping of Sinoatrial Node HCN Channel Expression in the Human Heart. *Circ Arrhythm Electrophysiol.* 2015;8:1219-1227.

4. Fedorov VV, Glukhov AV, Ambrosi CM, Kostecki G, Chang R, Janks D, Schuessler RB, Moazami N, Nichols CG, Efimov IR. Effects of KATP channel openers diazoxide and pinacidil in coronary-perfused atria and ventricles from failing and non-failing human hearts. *J Mol Cell Cardiol.* 2011;51:215-225.

5. Fedorov VV, Glukhov AV, Chang R, Kostecki G, Aferol H, Hucker WJ, Wuskell JP, Loew LM, Schuessler RB, Moazami N, Efimov IR. Optical mapping of the isolated coronary-perfused human sinus node. *J Am Coll Cardiol.* 2010;56:1386-1394.

6. Lou Q, Glukhov AV, Hansen B, Hage L, Vargos-Pinto P, Billman GE, Carnes CA, Fedorov VV. Tachy-brady arrhythmias: The critical role of adenosine-induced sino-atrial conduction block in post-tachycardia pauses. *Heart Rhythm.* 2013;10:110-118.

7. Lou Q, Hansen BJ, Fedorenko O, Csepe TA, Kalyanasundaram A, Li N, Hage LT, Glukhov AV, Billman GE, Weiss R, Mohler PJ, Gyorke S, Biesiadecki BJ, Carnes CA, Fedorov VV.

Upregulation of adenosine A1 receptors facilitates sinoatrial node dysfunction in chronic canine heart failure by exacerbating nodal conduction abnormalities revealed by novel dual-sided intramural optical mapping. *Circulation.* 2014;130:315-324.

8. Nixon BR, Thawornkaiwong A, Jin J, Brundage EA, Little SC, Davis JP, Solaro RJ, Biesiadecki BJ. AMP-activated protein kinase phosphorylates cardiac troponin I at Ser-150 to increase myofilament calcium sensitivity and blunt PKA-dependent function. *J Biol Chem.* 2012;287:19136-19147.

9. Voigt N, Trausch A, Knaut M, Matschke K, Varro A, Van Wagoner DR, Nattel S, Ravens U, Dobrev D. Left-to-right atrial inward rectifier potassium current gradients in patients with paroxysmal versus chronic atrial fibrillation. *Circ Arrhythm Electrophysiol.* 2010;3:472-480.

10. Brundel BJ, Van Gelder IC, Henning RH, Tuinenburg AE, Wietses M, Grandjean JG, Wilde AA, Van Gilst WH, Crijns HJ. Alterations in potassium channel gene expression in atria of patients with persistent and paroxysmal atrial fibrillation: differential regulation of protein and mRNA levels for K+ channels. *J Am Coll Cardiol.* 2001;37:926-932.

11. Zhao J, Hansen BJ, Csepe TA, Lim P, Wang Y, Williams M, Mohler PJ, Janssen P ML, Weiss R, Hummel JD, Fedorov VV. Intergration of High-Resolution Optical Mapping and 3-Dimensional Micro-Computed Tomographic Imaging to Resolve the Structure Basis of Atrial Conduction in the Human Heart. *Circulation Arrhythm Electrophysiol.* 2015;8:1514-1517.

12. Aslanidi OV, Nikolaidou T, Zhao J, Smaill BH, Gilbert SH, Holden AV, Lowe T, Withers PJ, Stephenson RS, Jarvis JC, Hancox JC, Boyett MR, Zhang H. Application of micro-computed tomography with iodine staining to cardiac imaging, segmentation, and computational model development. *IEEE Trans Med Imaging.* 2013;32:8-17.

13. Cabral HJ. Multiple Comparisons Procedures. *Circulation*. 2008;117:698-701